

PREPARED FOR SUBMISSION TO JCAP

Halo-Independent Direct Detection of Momentum-Dependent Dark Matter

John F. Cherry,¹ Mads T. Frandsen,² and Ian M. Shoemaker²

¹Theoretical Division, Los Alamos National Laboratory, Los Alamos, New Mexico 87545, USA

²CP³-Origins and the Danish Institute for Advanced Study, University of Southern Denmark, Campusvej 55, DK-5230 Odense M, Denmark

Abstract.

We show that the momentum dependence of dark matter interactions with nuclei can be probed in direct detection experiments without knowledge of the dark matter velocity distribution. This is one of the few properties of DM microphysics that can be determined with direct detection alone, given a signal of dark matter in multiple direct detection experiments with different targets. Long-range interactions arising from the exchange of a light mediator are one example of momentum-dependent DM. For data produced from the exchange of a massless mediator we find for example that the mediator mass can be constrained to be $\lesssim 10$ MeV for DM in the 20-1000 GeV range in a halo-independent manner.

Preprint numbers: [LA-UR-14-23073](#), [CP3-Origins-2014-018](#) [DNRF90](#), [DIAS-2014-18](#)

Contents

1	Introduction	1
2	Direct Detection in v_{\min}-space	2
3	Momentum-Dependent Dark Matter Scattering in v_{\min}-space: the \tilde{g} ratio test	3
4	Detector Mock-ups and Input Spectrum	6
5	Results	7
6	Conclusion	12
A	Signal Analysis	13
	A.1 Binned Maximum Likelihood	13
	A.2 Ratio Test	15

1 Introduction

A definitive, non-gravitational detection of Dark Matter (DM) has yet to occur. However a large number of low-background, direct searches for DM are underway with the goal of detecting the feeble nuclear recoil energy deposited by DM particles passing through the detector. The main target of these experiments are Weakly-Interacting Massive Particles (WIMPs), which are the most thoroughly studied DM candidates. The attractiveness of WIMP Dark Matter is driven by the fact that the relic abundance is controlled by their annihilation cross section. In the Early Universe, WIMPs are kept in thermal equilibrium by number-changing interactions, $\bar{X}X \leftrightarrow \bar{f}f$, where f is some SM particle. Eventually though, as the Universe expands and WIMPs are diluted, these number-changing interactions cease, and the abundance of WIMPs “freezes out.” Given that this paradigm requires DM to share some interactions with the SM, it provides many experimental lines of inquiry, and assuming that DM interacts with quarks or gluons it can be probed at direct detection experiments.

In view of the null results from direct detection and the LHC, simple models of thermal relic WIMPs termed Effective Field theory (EFT) models or ‘Maverick’ [1] models where the DM particle itself is the only new particle accessible at LHC, are nearly ruled out [2–4]. However, this conclusion is easily evaded when the EFT approach itself is not valid, as in the case of a mediator much lighter than the DM. Then annihilation of DM to a pair of mediators typically dominates over other available annihilation channels. In the case of asymmetric DM, the annihilation cross section requirement is even more stringent because one needs to “annihilate away” the symmetric abundance. Thus a light mediator coupling to DM remains a viable venue for symmetric or asymmetric DM.

In contrast with high-energy colliders, direct detection offers a sensitive probe of such light mediators at the cost of relying on the galactic DM halo to provide collisional energy. As a consequence of this direct detection experiments suffer from some uncertainty in the astrophysical distribution of DM. To combat this uncertainty, direct detection analysis using

astrophysics-independent methods for interpreting data has gained increased interest recently [5–10].

In the present paper, we illustrate the utility of these methods in determining the spin-independent of the DM scattering and outline a new method which is also agnostic with respect to the velocity distribution of DM in the halo. For simplicity we restrict this study to elastic, spin-independent scattering from single component DM. Using this simple method, we perform a projection study of what up-coming ton-scale experiments can say about the presence of light mediators, and more generally momentum dependence of the scattering cross section. Similar projections have been recently made for momentum-independent cross sections [11, 12] and momentum-dependent cross sections [13] assuming specific models of the DM velocity distribution.

2 Direct Detection in v_{\min} -space

Direct detection involves a combination of dark matter particle physics, nuclear physics and astrophysics. It has been pointed out that in the case of simple spin-independent interactions, one can “integrate out” the DM astrophysics and compare experiments without any assumptions about the unknown local DM distribution [6, 14]. These methods have since been extended to cover momentum-dependent [8] and inelastic scattering [15, 16].

For elastic, spin-independent scattering the differential scattering rate (not yet including detector effects) at a direct detection experiment is given by

$$\frac{dR}{dE_R} = \sum_j \mathcal{F}_j \frac{dR_j}{dE_R} = \sum_j \mathcal{F}_j \frac{1}{2\mu_{nX}^2} \left[\frac{f_p}{f_n} Z_j + (A_j - Z_j) \right]^2 F_j^2(E_R) \tilde{g}(v_{\min,j}), \quad (2.1)$$

where

$$\tilde{g}(v_{\min,j}) = \frac{\rho \sigma_n}{m_X} \int_{v_{\min,j}(E_R)}^{\infty} \frac{f(\mathbf{v} + \mathbf{v}_E(t))}{v} d^3v, \quad (2.2)$$

with σ_n the DM-neutron scattering cross section, m_X is the dark matter mass, the index j denotes the individual types of nuclide present in the detector medium with mass number A_j and proton number Z_j . \mathcal{F}_j is the number fraction of nuclide j , $F_j(E_R)$ is the nuclear form factor, μ_{nX} is the nucleon-DM reduced mass, f_p/f_n is the ratio of the effective proton and neutron couplings to DM [17].¹ Finally $f(\mathbf{v} + \mathbf{v}_E(t))$ is the local DM velocity distribution evaluated in the galactic rest frame and $\mathbf{v}_E(t)$ is the velocity of the Earth relative to the galactic rest frame.

The minimum velocity for an incoming DM particle to produce a nuclear recoil of energy E_R is

$$v_{\min,j}(E_R) = \sqrt{m_N E_R / 2\mu_j^2}, \quad (2.3)$$

with μ_j being the DM-nuclide reduced mass, and m_N is the mass of the nuclide. Lastly we also have in the above the astrophysics parameters ρ and $f(v)$ describing the local DM mass density and velocity distribution respectively. There is considerable uncertainty on these astrophysics parameters, and the DM inferences (e.g. its mass and scattering cross section) one naïvely draws from direct detection depend sensitively on their values.

¹Though we do not consider “isospin-violating” couplings in this paper, we note that both next-to-leading order effects [18, 19] and hadronic uncertainties [20] can be sizeable.

Rather than assuming the values of ρ and $f(v)$, we can instead report halo-independent constraints or parameter estimations on the quantities m_X , v_{\min} , and $\tilde{g}(v_{\min})$. Thus, assuming that $v_{\min,j}$ is independent of the nuclide, for each fixed DM mass m_X we can simply use the observed rate dR/dE_R to infer $\tilde{g}(v_{\min})$ as a function of v_{\min} :

$$\tilde{g}(v_{\min}) = \sum_j \frac{2\mu_{nX}^2}{\mathcal{F}_j [f_p/f_n Z_j + (A_j - Z_j)]^2 F_j^2(E_R)} \frac{dR_j}{dE_R}. \quad (2.4)$$

In performing such a mapping to v_{\min} -space in this way, we have assumed that the only momentum dependence in the scattering is in the nuclear form factor, where the relation between momentum transfer q and recoil energy is given by $q = \sqrt{2m_N E_R}$. We also assume that the experimenter has no ability to distinguish between recoils produced by different nuclides within the detector medium.

3 Momentum-Dependent Dark Matter Scattering in v_{\min} -space: the \tilde{g} ratio test

Let us now illustrate how a straightforward extension of this method can be used to extract information about the momentum dependence from direct detection data without making assumptions about the DM astrophysics. Here we aim for a qualitative discussion of the method and delay the introduction of detector effects such as finite energy resolution until Sec. 4.

Above in Eq.(2.4) we assumed that the energy-dependence from the DM microphysics is trivial, i.e. all the energy dependence is encoded in the nuclear form factor $F(E_R)$. There are many ways in which this assumption can be violated. An especially simple example, is that DM may exchange a very light mediator with nuclei. In this case, the cross section will scale as $d\sigma/dE_R \propto q^{-4}$. A simple parameterization [21] of non-trivial spin-independent is

$$\frac{d\sigma}{dE_R} = \left(\frac{d\sigma}{dE_R} \right)_0 \left(\frac{q^2}{q_{\text{ref}}^2} \right)^n \left(\frac{q_{\text{ref}}^2 + m_\phi^2}{q^2 + m_\phi^2} \right)^2, \quad (3.1)$$

where m_ϕ is the mass of the exchanged mediator, and we fix $q_{\text{ref}} = 10$ MeV throughout. Above, $(d\sigma/dE_R)_0$ is the standard spin-independent DM-nucleus cross section

$$\left(\frac{d\sigma}{dE_R} \right)_0 = \frac{m_N}{2\mu_{nX}^2 v^2} \tilde{\sigma}_n F^2(E_R). \quad (3.2)$$

Written in this way, the integer n parameterizes the unknown Lorentz structure of the DM-quark operator, while the momentum dependence from the propagator is explicitly factored out.² Thus the standard spin-independent contact interaction scattering corresponds to the $n = 0$, heavy mediator limit $m_\phi^2 \gg q^2$. The momentum transfer q is related to v_{\min} as $q = 2\mu v_{\min}$. Note that the quantity $\tilde{\sigma}_n$ is equal to the standard spin-independent cross section on neutrons only for $n = 0$ contact interactions. More generally the quantity $\tilde{\sigma}_n$ is a parameter with units of cross section which is a function of m_ϕ , q_{ref} , and n . The function of $\tilde{\sigma}_n$ is to fix the normalization of the rate for more complicated momentum-dependent interactions.

²We note that there are many interactions not described by Eq. (3.1) For example, DM magnetic dipole moment scattering contain multiple terms with differing momentum dependences. Moreover DM bound-state scattering or break-up [22] introduce additional sources of momentum dependence not encompassed by Eq.(3.1).

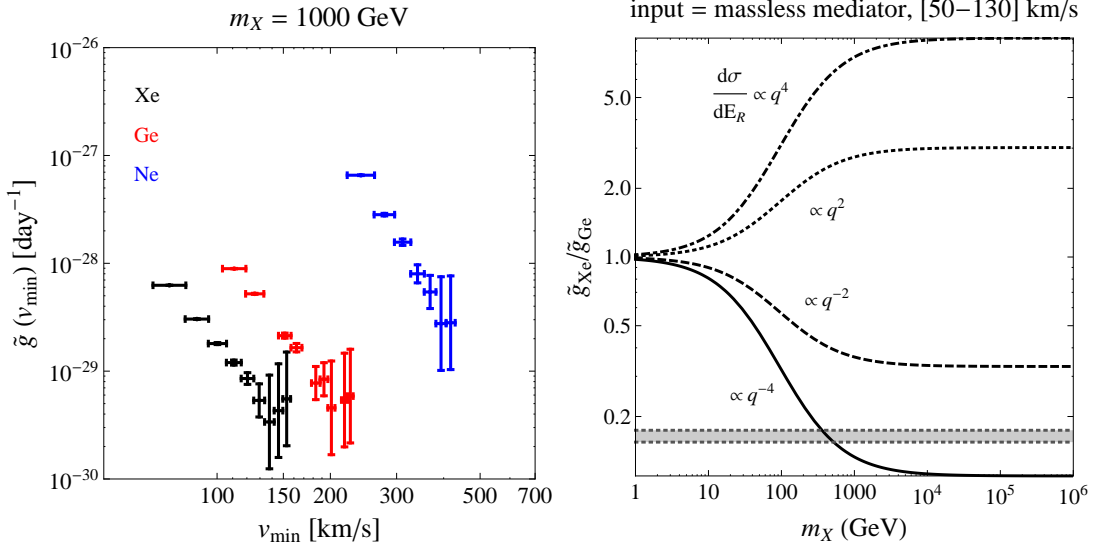


Figure 1. *Left:* Here the input data (from scattering via a massless mediator) is incorrectly mapped (assuming momentum-independent scattering) into $(\tilde{g} - v_{\min})$ space using Eq. (2.4). However where data bins overlap, the \tilde{g} ratios yield information about the momentum-dependence. *Right:* Expected \tilde{g} ratio between a Xe and Ge target in which DM scattering has a non-trivial spin-independent, parameterized by the integer n as shown in Eq. (3.1). The observed \tilde{g} ratio in a $[50 - 130]$ km/s bin is the shaded band.

With the simple cross section parameterization in Eq. (3.1) we are at first interested in distinguishing two possibilities: the presence or absence of momentum dependence in the DM interaction. To answer this question, we can simply use Eq. (3.1) with $m_\phi \gg q, q_{\text{ref}}$, such that the cross section becomes

$$\frac{d\sigma}{dE_R} = \left(\frac{d\sigma}{dE_R} \right)_0 \left(\frac{q^2}{q_{\text{ref}}^2} \right)^n. \quad (3.3)$$

In this case the signal of non-trivial momentum dependence corresponds to $n \neq 0$.

We now imagine the fortunate situation where two experiments employing different target materials observe a signal. If the dark matter microphysics is momentum-dependent, the data will lead to discrepant inferences of $\tilde{g}(v_{\min})$ under the assumption of Eq. (2.4). Suppose experiment i uses a target nucleus of mass m_{N_i} , $i = 1, 2$. With the signal spectrum produced from scattering of the type in Eq. (3.3), we expect experiment i to infer a value for $\tilde{g}(v_{\min})$ of

$$\tilde{g}_{\text{infer},i} = \tilde{g}_{\text{true}} \left(\frac{q^2}{q_{\text{ref}}^2} \right)^n = \tilde{g}_{\text{true}} \left(\frac{2\mu_i v_{\min}}{q_{\text{ref}}} \right)^{2n} \quad (3.4)$$

where $\mu_i = m_X m_{N_i} / (m_X + m_{N_i})$. Taking the ratio of the inferred value of $\tilde{g}(v_{\min})$ at the same v_{\min} by two different experiments we obtain (assuming spin-independent scattering³):

$$\left. \frac{\tilde{g}_{\text{infer},1}}{\tilde{g}_{\text{infer},2}} \right|_{v_{\min}} = \left(\frac{\mu_1}{\mu_2} \right)^{2n}. \quad (3.5)$$

³An analogous expression for spin-dependent scattering can be written down after constructing the \tilde{g}_{infer} using the spin-dependent form factor and average spin contributions from the proton and neutron spin groups.

At DM masses $m_X \gg m_{N_i}$ where $\mu_i \simeq m_{N_i}$, we expect a significant discrepancy to appear, implying momentum dependence of the true scattering cross-section. Instead at low DM masses $m_X \ll m_{N_i}$ when $\mu_i \simeq m_X$ and the momentum transfer is nearly identical for different targets, we expect little difference in the inferred values of \tilde{g} for different experiments and it will not be possible to distinguish between the above scenarios, e.g. [23].

We illustrate this in the left panel of Fig. 1, where we plot the ratio of the inferred values of $\tilde{g}(v_{\min})$ in Xenon, Germanium, and Neon experiments, using $m_X = 1000 \text{ GeV}$, $m_\phi = 0$, Eq. (3.1), and assuming Helm nuclear form factors. Thus at each value of v_{\min} that is compared, one expects an offset in the inferred value of \tilde{g} . The right hand panel of Fig. 1 illustrates the DM mass dependence of this offset, confirming that so long as we are not in the regime where $m_X \ll m_{N_i}$ momentum dependence will produce an offset that can be employed as a diagnostic of the momentum dependence of the scattering.

This simple \tilde{g} ratio measure is easily extended to include the mediator mass dependence by using Eq. (3.1) such that Eq.(3.5) generalizes to

$$\left. \frac{\tilde{g}_{\text{infer},1}}{\tilde{g}_{\text{infer},2}} \right|_{v_{\min}} = \left(\frac{\mu_1}{\mu_2} \right)^{2n} \left(\frac{4\mu_2^2 + (m_\phi/v_{\min})^2}{4\mu_1^2 + (m_\phi/v_{\min})^2} \right)^2. \quad (3.6)$$

Our strategy for determining the momentum dependence of the dark matter scattering is therefore to map the experimental data on dR/dE_R into bins in v_{\min} space and compare overlapping bins. In general, this mapping will be different for distinct experiments with different target nuclei and isotopic abundances, and will also depend on the hypothetical DM mass which we wish to test. This provides the benefit that our uncertainties on the velocity distribution of the DM in the galactic halo are guaranteed to cancel away when taking a ratio of two independent measurements. So long as the DM is single-component, the distinct experiments are guaranteed to sample precisely the same portion of the $\tilde{g}(v_{\min})$ curve. This provides a measurement of the DM interaction physics regardless of the de-facto shape of $\tilde{g}(v_{\min})$, provided that m_X is not so light that the DM-Nucleus reduced masses of all experiments are degenerate. In the case where no bins overlap we can, in principle, extrapolate a best fit curve of $\tilde{g}(v_{\min})$ through the available bins and then compare the inferred $\tilde{g}(v_{\min})$ functions. However this re-introduces dependence on the velocity function by way of forcing an observer to assume that the velocity distribution of the DM in the galactic halo corresponds to a known class of analytic functions (e.g. the Standard Halo Model) and the associated observational uncertainties.

Since we are interested in extracting the dependence of the cross-section on the momentum transfer, or equivalently the recoil energy, it is important to know the momentum dependence inherent in the nucleon and nuclear form factors. A general momentum dependence of the spin-independent differential dark matter-nucleus scattering on a given nuclide per unit time and detector mass, assuming a single DM species, may be written as [18]

$$\frac{dR}{dE_R} = \frac{\kappa_X \rho}{m_X} \int_0^\infty \left[\sum_i (f_p^i(q, v) F_p^i(q, v) Z + (A - Z) f_n^i(q, v) F_n^i(q, v) - T_2(q, v)) \right]^2 \frac{f(\mathbf{v} + \mathbf{v}_E(t))}{v} d^3v, \quad (3.7)$$

where κ_X is a factor specific to the nature of the DM particle, i runs over the exchanged mediators and we include both separate nuclear form factors $F_{n,p}^i(q, v)$ for protons and neutrons

target	ϵ_{eff} [ton \times yr]	E_{thr} [keV]	$\sigma(E)$ [keV]
Xe	0.88	5	$0.6 \text{ keV} \sqrt{E_R/\text{keV}}$
Ge	0.88	5	$\sqrt{(0.3)^2 + (0.06)^2 E_R/\text{keV}} \text{ keV}$
Ne	0.88	5	$1 \text{ keV} \sqrt{E_R/\text{keV}}$

Table 1. Characteristics of future direct dark matter experiments using Xenon, Germanium and Neon as target nuclei. Here ϵ_{eff} is the effective exposure, E_{thr} is the low-energy threshold, and $\sigma(E)$ is the energy resolution of the experiment.

and a form factor for two nucleon interactions $T_2(q, v)$ [18, 19] in addition to the single nucleon form factors $f_{p,n}^i(q, v)$. We also imagine a separation of $f_p^i(q) = f_{p,X}^i(q) f_{p,N}^i(q)$ where the first factor gives the particle physics momentum dependence of the interaction, arising from the DM-mediator vertex while the second factor gives the hadronic physics form factor. Thus in our example above in Eq. (3.3) we have assumed $f_{p,X}^i(q) = f_{n,X}^i(q) \sim q^{2n}$, $f_{n,N}^i(q) = f_{n,N}^i$, $T_2(q, v) = 0$ and an appropriate nuclear form factor $F_n^i(q, v) = F_p^i(q, v) = F(E_R)$.

For a scalar mediator, interacting with DM and quarks via Yukawa couplings with zero tree-level momentum dependence, the momentum-dependent part of $f_{n,p}(q)$ and $T_2(q, v)$ gives corrections to the rate of the order of a few percent below 100 keV nuclear recoil energies when the heavy quark couplings are suppressed, but can be large when unsuppressed [18, 19]. The same is true for the momentum dependence of the Helm form factor $F(E_R)$ and more importantly we expect differences between the Helm form factor (included in the analysis) and a more accurate form factor are not above this level. Extracting the momentum dependence from DM particle physics is therefore feasible.

We provide the details of our analysis below, and a complete description of our techniques in Appendix A.

4 Detector Mock-ups and Input Spectrum

To reasonably well simulate the near-term experimental capabilities, we include efficiencies, energy resolution, exposures, and background expectations. Similar theoretical projections have been made previously with momentum-independent [11, 12] and momentum-dependent cross sections [13] assuming specific models of the DM velocity distribution. We use 5 keV energy thresholds for Xenon, Germanium, and Neon targets. Given that large-scale xenon and germanium experiments with < 5 keV thresholds already exist, the adoption of 5 keV should be conservative. Although achieving such a low threshold for neon may be an experimental challenge, the results of the present paper motivate a low-mass target, low-threshold experiment.

For simplicity we shall assume Gaussian energy resolution. Though we note that this is not always the case in real detectors, we expect the correction to be small. The Gaussian energy resolution for each target is specified in Table 1. The number of events expected in the energy range $[E_1, E_2]$ is:

$$N(E_1, E_2) = \text{Exp} \int \text{Res}(E_1, E_2, E_R) \epsilon \frac{dR}{dE_R} dE_R, \quad (4.1)$$

where ϵ is the efficiency, Exp is the raw exposure (not including detector/analysis cut efficiencies), and $\text{Res}(E_1, E_2, E_R)$ is the detector response function taken to be

$$\text{Res}(E_1, E_2, E_R) = \frac{1}{2} \left[\text{erf} \left(\frac{E_2 - E_R}{\sqrt{2}\sigma(E_R)} \right) - \text{erf} \left(\frac{E_1 - E_R}{\sqrt{2}\sigma(E_R)} \right) \right]. \quad (4.2)$$

In this work we assume a raw exposure of 2.2 ton-years and a flat efficiency, $\epsilon = 0.4$, yielding an effective exposure of 0.88 ton-years unless otherwise stated. Lastly, we assume that each mock experiment will achieve their stated goals of reaching a < 1 background event expectation.

Though the velocity distribution remains unknown it has become canonical to assume a Maxwell-Boltzmann (MB) distribution [24, 25], truncated at the escape speed. We use this standard halo model (SHM) as our fiducial $f(v)$ choice to generate mock experimental spectra and note that detailed simulations of DM structure formation do not appear to deviate markedly from this choice [26].

In the rest frame of the Milky Way the velocity distribution,

$$f_{MB}(\vec{v}) = \begin{cases} N e^{-v^2/v_0^2}, & v < v_{esc} \\ 0, & v > v_{esc} \end{cases}, \quad (4.3)$$

is determined by its dispersion v_0 and the local escape speed v_{esc} . In this case the velocity integral $g(v_{\min})$ corresponding to the SHM has a closed form expression [17, 27–29].

In the SHM the dispersion is equated to the circular speed which is observable and measured to be $\langle v_e(t) \rangle = 230$ km/s [30, 31]. We use a local DM density $\rho_{DM} = 0.3$ GeVcm $^{-3}$ and escape speed $v_{esc} = 550$ km/s.

5 Results

To generate our mock signals, we have taken representative points in parameter space consistent with the LUX null results, specifically the 90% confidence limit upper bound on the DM-nucleon cross section [32]. The details of our LUX treatment can be found in [19, 33, 34]. Fits to the individual data sets for each detector medium are performed with standard Binned Maximum Likelihood (ML) analysis [35], which in addition to evaluating the goodness of fit for n , m_ϕ , and m_X optimizes the best fit in the velocity dispersion, v_0 , of the SHM. The individual datasets are then combined into a master dataset where the same ML analysis is performed for a “global” analysis. The details of this analysis can be found in Appendix A. Once these tests are complete, the \tilde{g} ratio test is also conducted on the original data set for every v_{\min} bin in which multiple experiments share observed events. Because we are exploring a three dimensional parameter space, we present the confidence interval data after it has been marginalized over one of the parameters (listed on the top of the figure with the true value of the parameter in the legend). When performing the marginalization procedure, we assume a flat prior for the entire parameter space.

As a first example, let us examine the results coming from the $m_X = 40$ GeV case with a massless mediator with $n = 0$. This would arise from the exchange of a light ($m_\phi \ll q$) vector or scalar. The marginalised $(1, 2, 3)\sigma$ best-fit contours are displayed in both the (m_ϕ, m_X) and (n, m_X) planes in the upper panel of Fig. 2. There we see that in addition to the benefit of having multiple targets with signal data, we also observe the utility of the \tilde{g} ratio test as defined in Sec. 3. In this example, the mediator mass is limited to a smaller upper bound of $m_\phi \lesssim 10$ MeV, while the operator integer is constrained to be $n < 0.2$, and the DM mass bounded to be $m_X = 40_{-8}^{+10}$ GeV. In this conservative example, we have shown that one can learn the DM mass while simultaneously learning that a new light force carrier connects DM and nuclei with an identifiable momentum dependence.

It is useful to know how general this conclusion is, and in particular if it holds for heavier DM. We simulate the situation of 10^3 GeV DM again interacting with a massless mediator

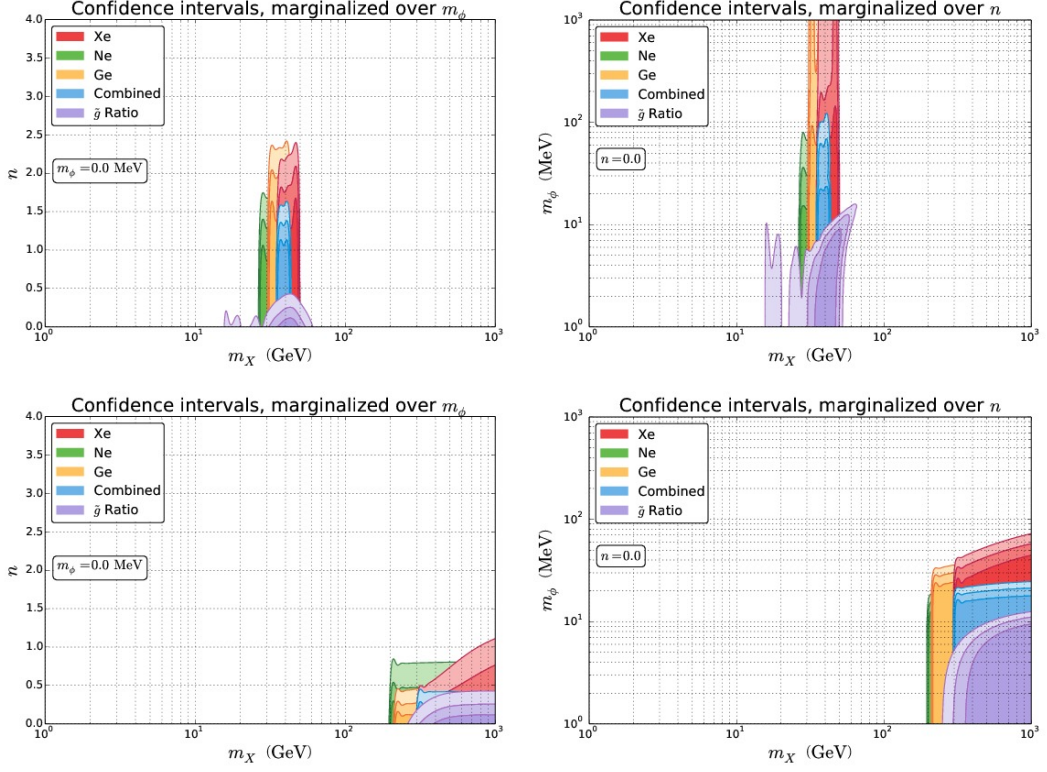


Figure 2. Reconstruction of DM parameters from an input spectrum generated via a massless mediator. The results on the first row correspond to DM mass $m_X = 20$ GeV, with $n = 0$, $\tilde{\sigma}_n = 3.8 \times 10^{-43}$ cm² and total event counts for each detector medium $\{N_{Ne} = 186, N_{Ge} = 123, N_{Xe} = 143\}$. The bottom row shows results for $m_X = 1000$ GeV, with $\tilde{\sigma}_n = 5.7 \times 10^{-42}$ cm² and total event counts for each detector medium $\{N_{Ne} = 178, N_{Ge} = 119, N_{Xe} = 87\}$. For each 2D plot the three parameters (n, m_X, m_ϕ) are fit to the mock data with one of the three parameters marginalized over. Figures on the left have been marginalized over m_ϕ and figures on the right have been marginalized over n . For each data set the 1, 2 and 3 σ confidence levels are shown from darkest to lightest shading respectively.

and display the results in the bottom panel of Fig. 2. Here only a lower bound on the DM mass $m_X \gtrsim 370$ GeV is possible. This is a result of a well-known $m_X - \sigma_n$ degeneracy at high DM mass that has been previously observed in spin-independent scattering (see e.g. [11, 36]), and arises simply from the fact that v_{\min} becomes independent of the DM mass at high m_X . Despite this degeneracy however both the mediator mass and operator integer remain well-constrained, $m_\phi \lesssim 90$ MeV, and $n \lesssim 0.2$ respectively.

As an example of possible degeneracies with our technique, we consider the possibility of inferring that DM-nucleon scattering contains no momentum dependence. An example of this sort with 100 GeV DM is shown in Fig. 3. Here we have chosen $n = 0$ and $m_\phi = 1$ GeV such that no relevant momentum dependence enters into the scattering cross section. There we observe that both the mass of the mediator and the operator integer n are not well-determined by the data. This degeneracy is linked to the phenomenon that a momentum-independent cross section could arise “accidentally” from the exchange of a light mediator with $n = 2$, c.f. Eq. (3.1), such that the two types of spin-independent cancel each other out. In this case the DM mass can be reliably reconstructed while the operator which produces the DM-quark

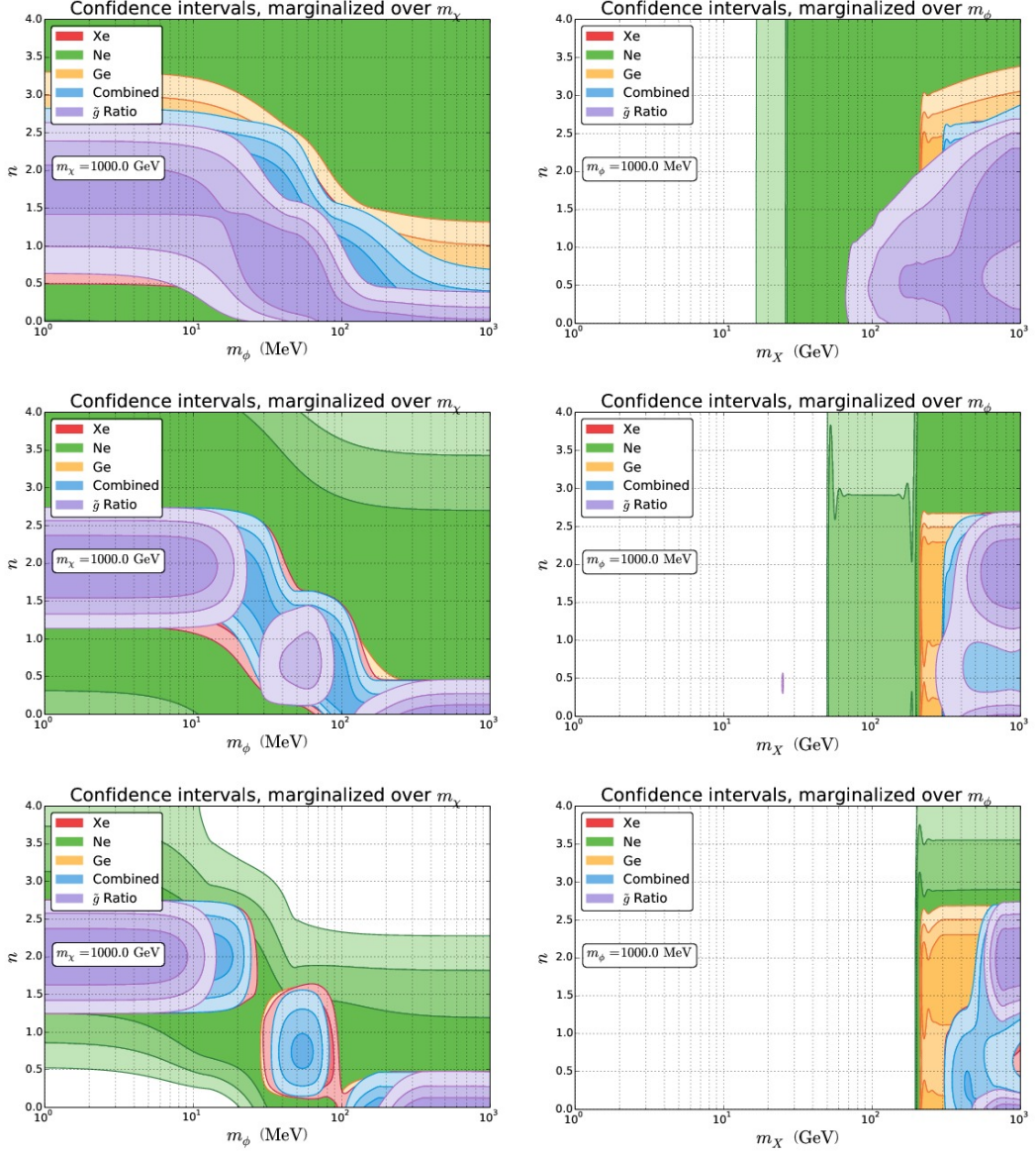


Figure 3. Reconstruction of DM parameters from an input spectrum generated via a contact interaction mediator. All results correspond to DM mass $m_X = 1000$ GeV, with $n = 0$, $m_\phi = 1000$ MeV, and $\tilde{\sigma}_n = 1.2 \times 10^{-44} \text{ cm}^2$. The total exposure time has been grouped by rows, increasing from top to bottom. The top row shows the confidence intervals for $\text{Exp} = 0.22 \text{ ton} \times \text{yr}$ and total event counts for each detector medium $\{N_{Ne} = 3, N_{Ge} = 39, N_{Xe} = 63\}$. The middle row shows the confidence intervals for $\text{Exp} = 0.88 \text{ ton} \times \text{yr}$ and total event counts for each detector medium $\{N_{Ne} = 10, N_{Ge} = 194, N_{Xe} = 276\}$. The bottom row shows the confidence intervals for $\text{Exp} = 3.52 \text{ ton} \times \text{yr}$ and total event counts for each detector medium $\{N_{Ne} = 43, N_{Ge} = 636, N_{Xe} = 1022\}$. Figures on the left have been marginalized over m_X and figures on the right have been marginalized over m_ϕ . For each data set the 1, 2 and 3 σ confidence levels are shown from darkest to lightest shading respectively.

interaction is limited to a pair-wise constraint (either $n = 0$ contact interaction or $n = 2$ with a massless mediator). Also shown in Figure 3 is the effect of increased effective exposure

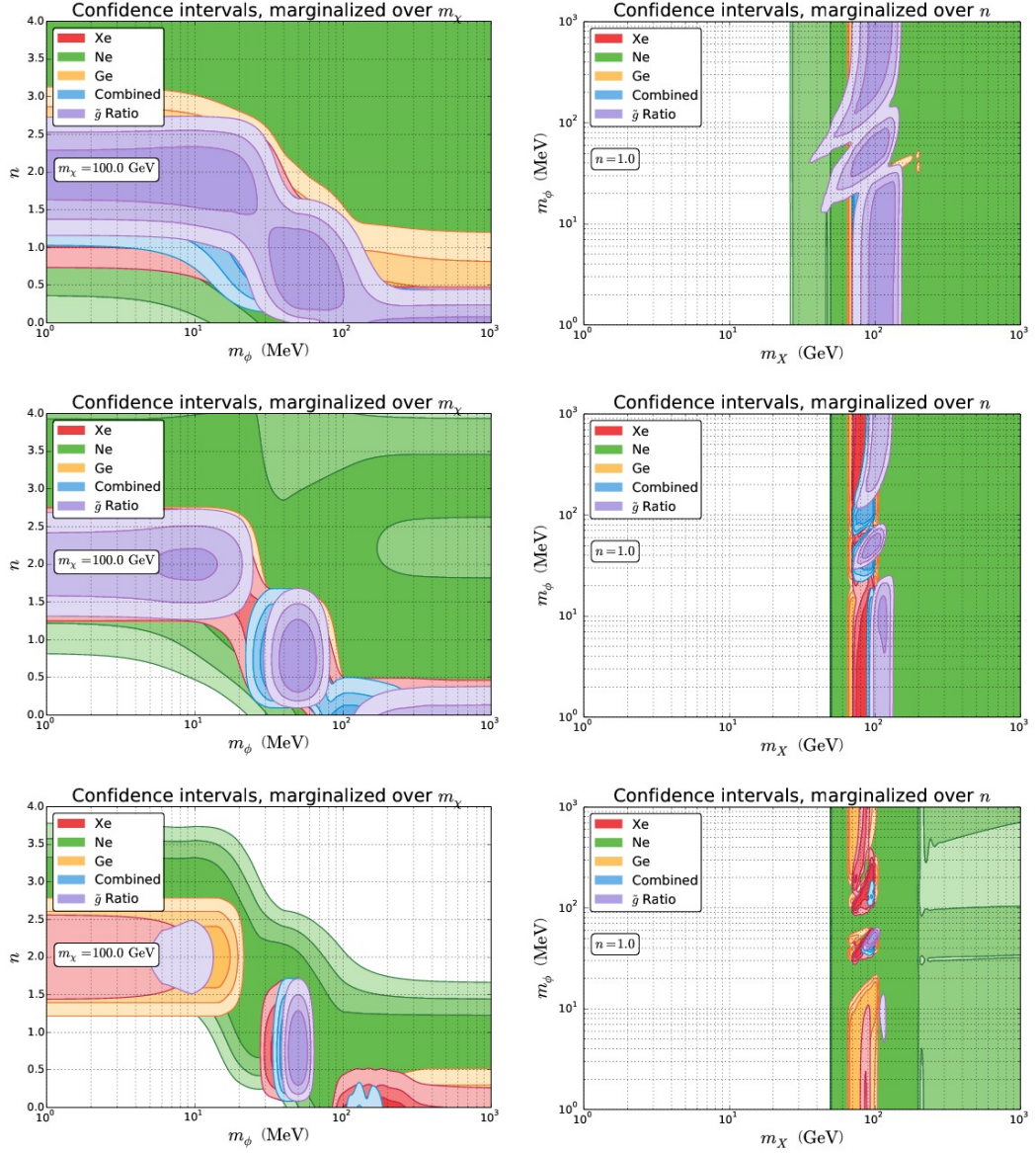


Figure 4. Reconstruction of DM parameters from an input spectrum generated via a intermediate mass mediator. All results correspond to DM mass $m_X = 100$ GeV, with $n = 1$, $m_\phi = 50$ MeV, and $\tilde{\sigma}_n = 2.7 \times 10^{-46} \text{ cm}^2$. The total exposure time has been grouped by rows, increasing from top to bottom. The top row shows the confidence intervals for $\text{Exp} = 0.88 \text{ ton} \times \text{yr}$ and total event counts for each detector medium $\{N_{Ne} = 9, N_{Ge} = 163, N_{Xe} = 254\}$. The middle row shows the confidence intervals for $\text{Exp} = 3.52 \text{ ton} \times \text{yr}$ and total event counts for each detector medium $\{N_{Ne} = 35, N_{Ge} = 650, N_{Xe} = 1017\}$. The bottom row shows the confidence intervals for $\text{Exp} = 14.08 \text{ ton} \times \text{yr}$ and total event counts for each detector medium $\{N_{Ne} = 143, N_{Ge} = 2601, N_{Xe} = 4073\}$. Figures on the left have been marginalized over m_X and figures on the right have been marginalized over m_ϕ . For each data set the 1, 2 and 3 σ confidence levels are shown from darkest to lightest shading respectively.

for the detectors. An additional degeneracy is present when there is insufficient data to rule out minor deviations in the inferred shape of $\tilde{g}(v_{\min})$. In such cases, a point in parameter

space which differs by $n = 1$ from the actual value is also possible. In the example shown here, $n = 1$ with $m_\phi \approx 45 \text{ MeV}$ is also a degenerate possibility, but one can see in Fig. 4 that this intermediate degeneracy is lifted with a sufficient number of events. If the DM-nucleon interaction is mediated by either a very light (or massless) or very massive mediator, one would need orthogonal data (e.g. collider or astrophysical) to infer which class of DM microphysics is truly responsible for the interaction.

Similar degeneracies in the inferred DM interaction parameters are present when intermediate mass mediators are considered. Figure 4 shows an example where $n = 1$, $m_\phi = 50 \text{ MeV}$, and $m_X = 100 \text{ GeV}$, so that typically $q \sim m_\phi$ for all experiments. The top panels of Fig. 4 exhibit similar degeneracies to those in Fig. 3. This is due to the similarity (within errors) of the overall shape of the $\tilde{g}(v_{\min})$ curve over the range where the experiments are capable of detecting recoils from DM interactions. The range of this degeneracy is limited to $n \pm 1$, which corresponds to a massless mediator ($n + 1$) or a contact interaction ($n - 1$). However, as can be seen in the bottom panels of Fig. 4, with a large number of observed events the statistical errors shrink to an extent which allows the degeneracy to be completely lifted.

To illustrate the true halo-independent character of the ratio test we show an example where the ML test and the ratio test were conducted for a DM velocity distribution which consisted of only 10 individual streams of DM. This is intended to mimic the intriguing possibility that the local DM distribution around Earth is dominated by several large streams as a consequence of the hierarchical structure formation of the Milky Way halo. The velocity profile was constructed from 10 streams which were randomly chosen via Monte Carlo from the probability distribution function of streams within the SHM. The prescription for finding a Monte Carlo probability distribution for the SHM is quite simple. We exploit the fact that the Maxwell-Boltzmann velocity distribution is a three dimensional Gaussian distribution in momentum space. This allows one to randomly generate dark matter stream momenta from the Gaussian distribution (which is cutoff above a certain momentum which corresponds to v_{esc} for a given dark matter mass) and convert those momenta to stream velocities. One then simply adds the velocity of the Earth about the galactic center to all of the stream velocity vectors and takes the resultant stream velocity magnitudes. We also assign a weight to each stream assuming a flat prior, as not all streams in the Milky Way halo are expected to contain the same quantity of dark matter. The sum of all weighted dark matter streams is then renormalized so that Monte Carlo realization is consistent with the LUX constraints on $\tilde{g}(v_{\min})$.

The SHM velocity profile used for the Monte Carlo realization followed the same parameters used throughout this paper, with $\langle v_e(t) \rangle = 230 \text{ km/s}$, $v_{esc} = 550 \text{ km/s}$, $v_0 = 230 \text{ km/s}$. An initial data set was prepared using $n = 2$, $m_X = 200 \text{ GeV}$, and $m_\phi = 50 \text{ MeV}$ using the 10 stream velocity distribution function. When performing the ML test, the goodness of fit was evaluated by optimizing the fit of the *continuous* SHM velocity profile to the observed data. The stochastic distribution of dark matter stream velocities results in isolated experiments being able to obtain good individual fits to the original microphysics of the DM, but the combined analysis of all observations rules out the entire interaction parameter space for DM with a confidence of $> 3\sigma$. In contrast, because the ratio test requires no assumption be made about the DM velocity distribution it is able to correctly identify the true DM interaction parameters as the best fit, along with the expected degeneracies between n and m_ϕ for a momentum-dependent cross section discussed above.

Lastly it is important to note that many models of DM interactions yield terms in the

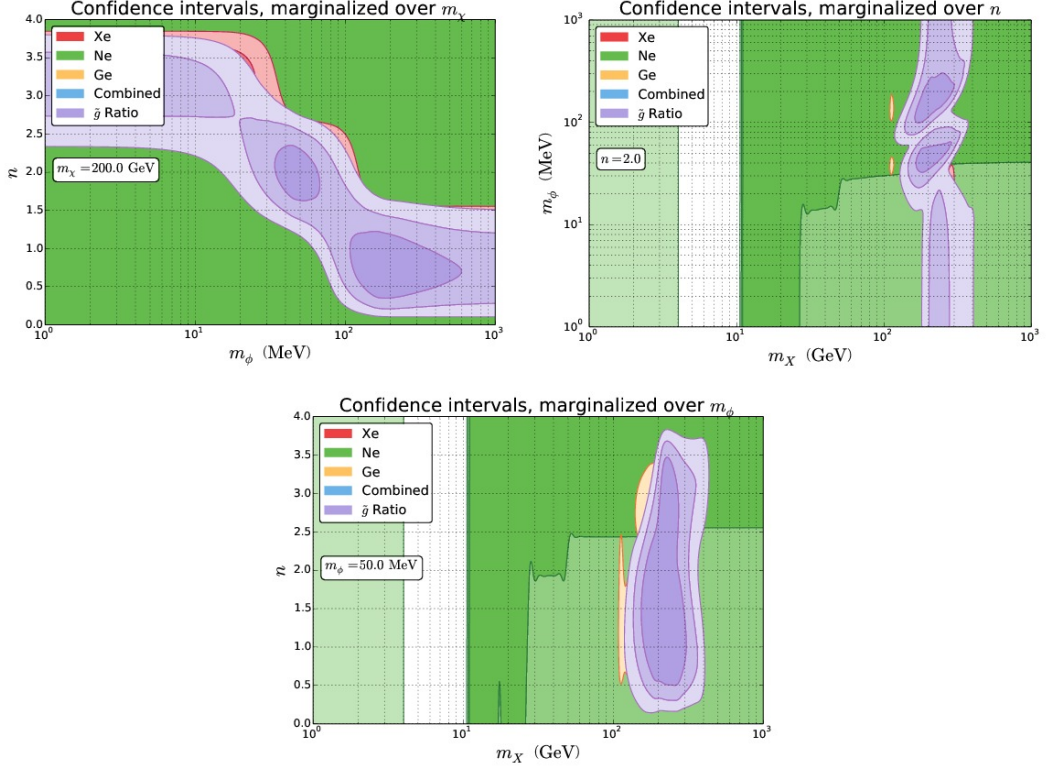


Figure 5. Reconstruction of DM parameters from an input velocity distribution which consisted of only 10 streams of dark matter. The velocity distribution was selected randomly via Monte Carlo from a probability distribution which matches the standard SHM velocity profile with $\langle v_e(t) \rangle = 230$ km/s, $v_{esc} = 550$ km/s, $v_0 = 230$ km/s. The ML analysis was conducted under the assumption of a continuous SHM velocity distribution which has the same parameters. The results were generated using the dark matter interaction parameters $n = 2$, $m_X = 200$ GeV, and $m_\phi = 50$ MeV, with $\tilde{\sigma}_n = 1.0 \times 10^{-47}$ cm² and total event counts for each detector medium $\{N_{Ne} = 1, N_{Ge} = 145, N_{Xe} = 333\}$. Note that because of the small number of streams which dominate the dark matter velocity distribution, the ML analysis *rules out* the entire DM interaction parameter space with a confidence of $> 3\sigma$ for the combined fit. For each data set the 1, 2 and 3 σ confidence levels are shown from darkest to lightest shading respectively.

cross section with disparate momentum dependence. However even in the case that multiple terms with different q dependences enter, the method illustrated presently would yield a determination of some non-integer value of n . Beyond such a determination, we leave the extension of this method to more general spin-independent for future work.

6 Conclusion

We have presented and illustrated a new method for determining the momentum dependence of DM from direct detection data in a genuinely halo-independent manner. In many cases the momentum dependence of the DM-nucleus scattering cross section can be well-determined from future direct detection data. The complementarity of targets aids significantly in this determination. Moreover, it is worth stressing again that this is one of the few properties

of dark matter microphysics that can be extracted from near-term experiments in a manner that is independent of the DM velocity distribution. This does not necessarily hold for the velocity-dependence of the scattering, which may be degenerate with the form of the velocity distribution and require different techniques to be robustly determined.

As we have argued, one especially interesting application of these methods is their ability to reveal the existence of a new light force carrier between DM and nuclei. Such mediators have been invoked both in the context of evading collider and direct detection limits while retaining a sufficiently large annihilation cross section to be a thermal relic. Moreover such mediators could be relevant for the self-scattering of DM [37–39].

Acknowledgements

We would like to thank Andreas Crivellin, Eugenio Del Nobile, Martin Hoferichter, Ranjan Laha, and Stefano Scopel for useful comments. The CP3-Origins centre is partially funded by the Danish National Research Foundation, grant number DNRF90. MTF acknowledges a Sapere Aude Grant no. 11-120829 from the Danish Council for Independent Research. This work was also supported in part by the U.C. Office of the President in conjunction with the LDRD Program at LANL.

A Signal Analysis

Now that we have established the basic ingredients which create a dark matter signal in our suite of next generation detectors, we must endeavor to determine what sort of information might be extracted from such a signal. We are primarily interested in extracting constraints on the momentum dependence n of the dark matter interaction with ordinary nuclear matter. It is also possible that one might infer limits on the dark matter mass and the mass of the mediator which couples DM and quarks from the halo-independent parameterization of $\tilde{g}(v_{\min})$, in addition to the momentum dependence of the interaction.

A.1 Binned Maximum Likelihood

In order to compute the expected number of events for each experiment we must specify a velocity distribution. We follow the notation of [28] for the SHM where the dispersion, escape speed, and boost velocity from the Galactic to Earth frame are respectively v_0 , v_{esc} , and v_{obs} . We will refer to the synthetic observed data as $\{x_i\}$, which is the set of counts x in bin i of a given experiment (all x_i are natural numbers). Once the simulated signal has been generated for a given detector (outlined in Section 4) our task turns to the business of constraining what range of dark matter interaction parameters produce a good fit to the data. We choose to vary the momentum dependence, n , dark matter mass m_X , and the interaction mediator mass m_ϕ over the parameter space.

To evaluate the goodness of fit for each choice of parameters we generate a new set of synthetic data $\{\mu_i\}$, which is the set of expected events μ in bin i of an experiment under the assumption that the point in parameter space we have selected is the *correct* one. Once we have chosen a given trio of n , m_X , and m_ϕ and generated our expected $\{\mu_i\}$, this allows us to normalize the overall dark matter cross section, σ_X , by scaling the predicted number of events, $\sum_i \{\mu_i\}$, to match total number of events in the simulated data set, $\sum_i \{x_i\}$. The normalization of the dark matter cross section is performed independently for each of the three detector media. Our intent is to mimic the actions of independently operated detection

experiments, which would reasonably choose to first analyze the data in their own detector as an isolated set of events.

Having generated an expected signal $\{\mu_i\}$ we then compare the simulated signal data $\{x_i\}$ for a given detector to the null hypothesis for the expected signal. Explicitly we evaluate the probability that the observed data $\{x_i\}$ is a statistical fluctuation on the expected event count $\{\mu_i\}$ for the fixed parameters n , m_X , and m_ϕ . This probability is then interpreted as our goodness of fit with which a given point in our parameter space matches the observed data and used to define the confidence intervals shown in the figures in the preceding sections.

The general prescription for this analysis is known as the Binned Maximum Likelihood method [35]. We begin with the Poisson probability, P_i , for each bin in the data to match the expected number of events,

$$P_i = \frac{\mu_i^{x_i}}{x_i!} e^{-\mu_i}. \quad (\text{A.1})$$

The likelihood, L , of observing the signal $\{x_i\}$ with expectation $\{\mu_i\}$ is given by the product of the Poisson probabilities,

$$L(\{x_i\}, \{\mu_i\}) = \prod_i P_i = \prod_i \frac{\mu_i^{x_i}}{x_i!} e^{-\mu_i}. \quad (\text{A.2})$$

The probability distribution of L for different sets of $\{x_i\}$ is invariant when Eq. (A.2) is multiplied by an overall constant. For reasons which will become clear shortly, we will choose to multiply Eq. (A.2) by $L^{-1}(\{x_i\}, \{x_i\})$. This will allow us to make the convenient definition of the likelihood ratio,

$$\mathcal{L}(\{x_i\}, \{\mu_i\}) = -\ln \left[\frac{L(\{x_i\}, \{\mu_i\})}{L(\{x_i\}, \{x_i\})} \right]. \quad (\text{A.3})$$

With a bit of algebra it can be shown that the likelihood ratio has a simple form,

$$\mathcal{L}(\{x_i\}, \{\mu_i\}) = \sum_i \mu_i - x_i + x_i \ln \frac{x_i}{\mu_i}, \quad (\text{A.4})$$

which is much simpler to evaluate than Eqs. (A.2) or (A.3) and has the benefit of being a positive number for all realizations of the expectation $\{\mu_i\}$. An important property of \mathcal{L} is that in the limit of “large” $\{x_i\}$ the likelihood ratio probability distribution asymptotes to the χ^2 probability distribution, with the relation that $\mathcal{L} \simeq \chi^2/2$, a result known as Wilks’ Theorem [40].

The goodness of fit for the point in parameter space we are considering can be determined by comparing $\mathcal{L}(\{x_i\}, \{\mu_i\})$ to cumulative probability distribution function of \mathcal{L} to compute the probability that the observed events satisfy the null hypothesis. Generally, there is no closed analytic form for the cumulative probability distribution function of \mathcal{L} (although one might use the closed form of the χ^2 distribution if there are a sufficiently large number of events for Wilk’s Theorem to apply), so the distribution function must be constructed via Monte Carlo methods.

We begin by computing $\{x'_i\}$, a Monte Carlo realization of the expected data set $\{\mu_i\}$ constructed using the Poisson probability in Eq. (A.1). For this new data set, we compute $\mathcal{L}(\{x'_i\}, \{\mu_i\})$ and record the value in a histogram. Repeating this procedure many times will build up the probability distribution of \mathcal{L} empirically. For this work we compute up to the 3σ confidence intervals for our synthetic data sets. This requires $P(3\sigma) \geq 1/\sqrt{N}$, where N

is the number of Monte Carlo realizations we create to compute the probability distribution function, yielding $N \geq 1.4 \times 10^5$ realizations.

In addition to evaluating the goodness of fit for the hypothetical Ne, Ge, and Xe detectors, we also evaluate the combined goodness of fit to all of the experimental data sets. This is done simply by repeating the steps outlined in the preceding three paragraphs for the combined data set $\{x_j^{combined}\} = \{\{x_i^{Ne}\}, \{x_i^{Ge}\}, \{x_i^{Xe}\}\}$, with the associated combined predicted number of events $\{\mu_j^{combined}\} = \{\{\mu_i^{Ne}\}, \{\mu_i^{Ge}\}, \{\mu_i^{Xe}\}\}$.

A.2 Ratio Test

There is an additional test which provides improved diagnostics of the microphysics governing the dark matter nucleon interaction which is possible only when comparing two or more experiments which have distinct detection media. We begin by supposing that there is only a single species of dark matter which is detected by our suite of experiments. This is by no means a certainty, but for our purposes the introduction of multi-component dark matter would produce undue complexity which is not motivated by current observational constraints. With single component dark matter, we can say concretely that there can be only one dark matter velocity distribution which is sampled by all of the experiments, $\tilde{g}_{true}(v_{min})$. However, in the instance that the momentum dependence of the dark matter interaction is a free parameter, the reconstructed function $\tilde{g}_{infer}(v_{min})$ is modified by both the reduced mass of the dark matter-nucleus system and the momentum dependence of the dark matter interaction, i.e. Equation (3.1). By proceeding bin by bin and comparing the overall normalization of $\tilde{g}_{infer}(v_{min})$ from detectors which employ different media, we can derive a constraint on the allowed ratio of $\tilde{g}_{infer}(v_{min})$ between the two experiments. One can choose to compare the ratio of $\tilde{g}_{infer,1}/\tilde{g}_{infer,2}$, which is shown in Equation (3.6), or to reconstruct $\tilde{g}_{true,1}(v_{min})/\tilde{g}_{true,2}(v_{min})$ under a chosen set of DM interaction parameters and verify that the ratio is equal to unity. Both of these techniques are equivalent and together they define what we call the “Ratio” test, wherein the reconstructed $\tilde{g}(v_{min})$ functions from multiple distinct experiments must satisfy the requirement that all experiments observe the same velocity distribution self-consistently.

To begin with we take the synthetic events, $\{x_i\}$, for each detector medium which are already binned identically in v_{min} for a specific choice of m_X according to Equation (2.3). This organization ensures that the data sets for all of the experiments, $\{x_i^{Ne}\}, \{x_i^{Ge}\}, \{x_i^{Xe}\}$, share bins which sample identical regions of the velocity space. For each bin of the data sets which contains observed events we obtain an inference of $\langle \tilde{g}(v_{min}) \rangle_i$ within that bin by taking the value of \tilde{g} to be constant over the bin width, $\Delta v_{min} = v_{min,2} - v_{min,1}$, so that for bin i ,

$$x_i = \langle \tilde{g}(v_{min}) \rangle_i \text{Exp} \sum_j \mathcal{F}_j \int_0^\infty \frac{[f_p/f_n Z_j + (A_j - Z_j)]^2 F_j^2(E_R)}{2\mu_{nX}^2} \text{Res}(E_{1,j}, E_{2,j}, E_R) \times \epsilon \left(\frac{q_j^2(E_R)}{q_{ref}^2} \right)^n \left(\frac{q_{ref}^2 + m_\phi^2}{q_j^2(E_R) + m_\phi^2} \right)^2 dE_R, \quad (\text{A.5})$$

where again the index j denotes the target nuclide with number fraction \mathcal{F}_j , and $E_{1,j}$, $E_{2,j}$ are the j^{th} nuclide’s recoil energy bin thresholds which correspond to the original v_{min} bin thresholds $v_{min,1}$, $v_{min,2}$. Eq. (A.5) can then be reversed to obtain $\langle \tilde{g}(v_{min}) \rangle_i$ for each bin of our synthetic data sets. Note that whether one recovers $\langle \tilde{g}_{true}(v_{min}) \rangle$ or $\langle \tilde{g}_{infer}(v_{min}) \rangle$ from Equation (A.5) depends on if the DM momentum-dependent interaction physics is included

(shown above) or excluded (by setting all momentum transfer dependent terms equal to unity), respectively.

Once the full set of data has been converted into a set of measured $\langle \tilde{g}(v_{\min}) \rangle$, $\{\langle \tilde{g}_i^{Ne} \rangle\}$, $\{\langle \tilde{g}_i^{Ge} \rangle\}$, $\{\langle \tilde{g}_i^{Xe} \rangle\}$, we can compute the ratio of \tilde{g} 's in overlapping v_{\min} bins. We employ the assumption of Poisson random noise in each bin to derive the statistical error associated with the computed ratio, which is then simply the addition in quadrature of the fractional error associated with each individual data bin in the ratio. This procedure produces a set of three ratio data sets $\{\{R_i^{Ne/Xe}\}, \{R_i^{Ne/Ge}\}, \{R_i^{Ge/Xe}\}\}$ and associated uncertainties $\{\{\sigma_i^{Ne/Xe}\}, \{\sigma_i^{Ne/Ge}\}, \{\sigma_i^{Ge/Xe}\}\}$. The expected values of these ratios, $\{\{\rho_i^{Ne/Xe}\}, \{\rho_i^{Ne/Ge}\}, \{\rho_i^{Ge/Xe}\}\}$, can be computed easily from Equation (3.6) if the \tilde{g}_{infer} ratio is used. If the \tilde{g}_{true} ratio is used, the expected value for all $\mu_i \equiv 1$. The χ^2 value of the ratio test for a fixed point in the m_X , m_ϕ , n parameter space is then computed directly for the entire data set, along with the accompanying statistical significance.

It is important to note that this procedure does introduce a systematic error into the inferred values of $\langle \tilde{g}(v_{\min}) \rangle$ which is dependent on both the detector response details and the actual distribution of dark matter velocities in the galactic halo $\tilde{g}_{actual}(v_{\min})$. This error arises directly from the approximation inherent in Eq. (A.5) that over the width of a v_{\min} bin the function $\tilde{g}(v_{\min})$ is constant. However, the true average of $\tilde{g}_{actual}(v_{\min})$ over this range is given by,

$$\langle \tilde{g}_{actual}(v_{\min}) \rangle = \frac{1}{\Delta v_{\min}} \int_{v_{\min,1}}^{v_{\min,2}} \tilde{g}_{actual}(v'_{\min}) dv'_{\min}. \quad (\text{A.6})$$

This leads to the overall systematic error in each determination of $\langle \tilde{g}(v_{\min}) \rangle$ of,

$$\sigma_{sys} = \langle \tilde{g}(v_{\min}) \rangle - \langle \tilde{g}_{actual}(v_{\min}) \rangle. \quad (\text{A.7})$$

Empirically, we have found that this additional systematic error is sub-dominant to the statistical error present in our synthetic samples. Statistically, typical fractional errors in the ratio test are $\sigma_i/R_i \sim O(1-0.1)$, which arises from taking the exposure, $\text{Exp} = .88 \text{ ton} \times \text{yr}$, along with the LUX limits on the dark matter interaction cross sections. None of our mock experiments are projected to have more than ~ 100 events per bin. For comparison, the typical fractional error which is introduced systematically by our approach is $\sigma_{sys}/\langle \tilde{g}_{actual}(v_{\min}) \rangle \sim O(0.01)$. This is easily understood from the form of the SHM velocity distribution function, which is regular and devoid of sharp features. Thus, for a sufficiently narrow v_{\min} bin the function $\tilde{g}(v_{\min})$ is linearizable over the bin width and asymptotically $\langle \tilde{g}(v_{\min}) \rangle - \langle \tilde{g}_{actual}(v_{\min}) \rangle \rightarrow 0$. This is somewhat idealized, however, as finite detector resolution effects will preclude the value of σ_{sys} from reaching this asymptotic value when the width of v_{\min} bin becomes comparable to the detector resolution.

References

- [1] M. Beltran, D. Hooper, E. W. Kolb, Z. A. Krusberg, and T. M. Tait, *Maverick dark matter at colliders*, *JHEP* **1009** (2010) 037, [[arXiv:1002.4137](#)].
- [2] J. Goodman, M. Ibe, A. Rajaraman, W. Shepherd, T. M. Tait, et al., *Constraints on Light Majorana dark Matter from Colliders*, *Phys.Lett.* **B695** (2011) 185–188, [[arXiv:1005.1286](#)].

- [3] Y. Bai, P. J. Fox, and R. Harnik, *The Tevatron at the Frontier of Dark Matter Direct Detection*, *JHEP* **1012** (2010) 048, [[arXiv:1005.3797](#)].
- [4] P. J. Fox, R. Harnik, J. Kopp, and Y. Tsai, *Missing Energy Signatures of Dark Matter at the LHC*, *Phys.Rev.* **D85** (2012) 056011, [[arXiv:1109.4398](#)].
- [5] M. Drees and C.-L. Shan, *Model-Independent Determination of the WIMP Mass from Direct Dark Matter Detection Data*, *JCAP* **0806** (2008) 012, [[arXiv:0803.4477](#)].
- [6] P. J. Fox, J. Liu, and N. Weiner, *Integrating Out Astrophysical Uncertainties*, *Phys.Rev.* **D83** (2011) 103514, [[arXiv:1011.1915](#)].
- [7] M. T. Frandsen, F. Kahlhoefer, C. McCabe, S. Sarkar, and K. Schmidt-Hoberg, *Resolving astrophysical uncertainties in dark matter direct detection*, *JCAP* **1201** (2012) 024, [[arXiv:1111.0292](#)].
- [8] E. Del Nobile, G. Gelmini, P. Gondolo, and J.-H. Huh, *Generalized Halo Independent Comparison of Direct Dark Matter Detection Data*, *JCAP* **1310** (2013) 048, [[arXiv:1306.5273](#)].
- [9] B. Feldstein and F. Kahlhoefer, *A new halo-independent approach to dark matter direct detection analysis*, [arXiv:1403.4606](#).
- [10] P. J. Fox, Y. Kahn, and M. McCullough, *Taking Halo-Independent Dark Matter Methods Out of the Bin*, [arXiv:1403.6830](#).
- [11] M. Pato, L. Baudis, G. Bertone, R. Ruiz de Austri, L. E. Strigari, et al., *Complementarity of Dark Matter Direct Detection Targets*, *Phys.Rev.* **D83** (2011) 083505, [[arXiv:1012.3458](#)].
- [12] M. Pato, L. E. Strigari, R. Trotta, and G. Bertone, *Taming astrophysical bias in direct dark matter searches*, *JCAP* **1302** (2013) 041, [[arXiv:1211.7063](#)].
- [13] S. D. McDermott, H.-B. Yu, and K. M. Zurek, *The Dark Matter Inverse Problem: Extracting Particle Physics from Scattering Events*, *Phys.Rev.* **D85** (2012) 123507, [[arXiv:1110.4281](#)].
- [14] P. J. Fox, G. D. Kribs, and T. M. Tait, *Interpreting Dark Matter Direct Detection Independently of the Local Velocity and Density Distribution*, *Phys.Rev.* **D83** (2011) 034007, [[arXiv:1011.1910](#)].
- [15] N. Bozorgnia, J. Herrero-Garcia, T. Schwetz, and J. Zupan, *Halo-independent methods for inelastic dark matter scattering*, *JCAP* **1307** (2013) 049, [[arXiv:1305.3575](#)].
- [16] S. Scopel and K. Yoon, *A systematic halo-independent analysis of direct detection data within the framework of Inelastic Dark Matter*, [arXiv:1405.0364](#).
- [17] G. Jungman, M. Kamionkowski, and K. Griest, *Supersymmetric dark matter*, *Phys.Rept.* **267** (1996) 195–373, [[hep-ph/9506380](#)].
- [18] V. Cirigliano, M. L. Graesser, and G. Ovanesyan, *WIMP-nucleus scattering in chiral effective theory*, *JHEP* **1210** (2012) 025, [[arXiv:1205.2695](#)].
- [19] V. Cirigliano, M. L. Graesser, G. Ovanesyan, and I. M. Shoemaker, *Shining LUX on Isospin-Violating Dark Matter Beyond Leading Order*, [arXiv:1311.5886](#).
- [20] A. Crivellin, M. Hoferichter, and M. Procura, *Accurate evaluation of hadronic uncertainties in spin-independent WIMP-nucleon scattering: Disentangling two- and three-flavor effects*, *Phys.Rev.* **D89** (2014) 054021, [[arXiv:1312.4951](#)].
- [21] S. Chang, A. Pierce, and N. Weiner, *Momentum Dependent Dark Matter Scattering*, *JCAP* **1001** (2010) 006, [[arXiv:0908.3192](#)].
- [22] R. Laha and E. Braaten, *Direct detection of dark matter in universal bound states*, *Phys.Rev.* **D89** (2014) 103510, [[arXiv:1311.6386](#)].

- [23] M. T. Frandsen, F. Kahlhoefer, C. McCabe, S. Sarkar, and K. Schmidt-Hoberg, *The unbearable lightness of being: CDMS versus XENON*, *JCAP* **1307** (2013) 023, [[arXiv:1304.6066](#)].
- [24] A. Drukier, K. Freese, and D. Spergel, *Detecting Cold Dark Matter Candidates*, *Phys.Rev.* **D33** (1986) 3495–3508.
- [25] K. Freese, J. A. Frieman, and A. Gould, *Signal Modulation in Cold Dark Matter Detection*, *Phys.Rev.* **D37** (1988) 3388.
- [26] M. Kuhlen, N. Weiner, J. Diemand, P. Madau, B. Moore, et al., *Dark Matter Direct Detection with Non-Maxwellian Velocity Structure*, *JCAP* **1002** (2010) 030, [[arXiv:0912.2358](#)].
- [27] P. Smith and J. Lewin, *Dark Matter Detection*, *Phys.Rept.* **187** (1990) 203.
- [28] C. Savage, K. Freese, and P. Gondolo, *Annual Modulation of Dark Matter in the Presence of Streams*, *Phys.Rev.* **D74** (2006) 043531, [[astro-ph/0607121](#)].
- [29] C. McCabe, *The Astrophysical Uncertainties Of Dark Matter Direct Detection Experiments*, *Phys.Rev.* **D82** (2010) 023530, [[arXiv:1005.0579](#)].
- [30] J. Bovy, D. W. Hogg, and H.-W. Rix, *Galactic masers and the Milky Way circular velocity*, *Astrophys.J.* **704** (2009) 1704–1709, [[arXiv:0907.5423](#)].
- [31] P. J. McMillan and J. J. Binney, *The uncertainty in Galactic parameters*, [arXiv:0907.4685](#).
- [32] **LUX Collaboration** Collaboration, D. Akerib et al., *First results from the LUX dark matter experiment at the Sanford Underground Research Facility*, [arXiv:1310.8214](#).
- [33] M. T. Frandsen, F. Sannino, I. M. Shoemaker, and O. Svendsen, *LUX Constraints on Magnetic Dark Matter in the $SE\bar{\chi}\chi$ Model with(out) Naturality*, [arXiv:1312.3326](#).
- [34] M. T. Frandsen and I. M. Shoemaker, *The Up-Shot of Inelastic Down-Scattering at CDMS-Si*, [arXiv:1401.0624](#).
- [35] J. Beringer and e. (Particle Data Group), *Review of Particle Physics (RPP)*, *Phys. Rev. D* **86** (2012) 010001.
- [36] A. Friedland and I. M. Shoemaker, *Integrating In Dark Matter Astrophysics at Direct Detection Experiments*, *Phys.Lett.* **B724** (2013) 183–191, [[arXiv:1212.4139](#)].
- [37] J. L. Feng, M. Kaplinghat, and H.-B. Yu, *Halo Shape and Relic Density Exclusions of Sommerfeld-Enhanced Dark Matter Explanations of Cosmic Ray Excesses*, *Phys.Rev.Lett.* **104** (2010) 151301, [[arXiv:0911.0422](#)].
- [38] A. Loeb and N. Weiner, *Cores in Dwarf Galaxies from Dark Matter with a Yukawa Potential*, *Phys.Rev.Lett.* **106** (2011) 171302, [[arXiv:1011.6374](#)].
- [39] S. Tulin, H.-B. Yu, and K. M. Zurek, *Beyond Collisionless Dark Matter: Particle Physics Dynamics for Dark Matter Halo Structure*, *Phys.Rev.* **D87** (2013) 115007, [[arXiv:1302.3898](#)].
- [40] S. S. Wilks, *The Large-Sample Distribution of the Likelihood Ratio for Testing Composite Hypotheses*, *The Annals of Mathematical Statistics* **9** (1938) 60–62.